First-principles study of methane dehydrogenation on a bimetallic Cu/N(111) surface

ARTICLE *in* THE JOURNAL OF CHEMICAL PHYSICS · NOVEMBER 2009

Impact Factor: 2.95 · DOI: 10.1063/1.3254383 · Source: PubMed

3 AUTHORS, INCLUDING:

Wei An
Shanghai University of Engineering Science
47 PUBLICATIONS **1,064** CITATIONS

SEE PROFILE

First-principles study of methane dehydrogenation on a bimetallic Cu/N(111) surface

Wei An* Xiao Cheng Zeng†

C. Heath Turner‡

*University of Alabama

†University of Nebraska-Lincoln, xzeng1@unl.edu

‡University of Alabama

First-principles study of methane dehydrogenation on a bimetallic Cu/Ni(111) surface

Wei An,[1,a)] X. C. Zeng,[2,b)] and C. Heath Turner[1,c)]
[1]*Department of Chemical and Biological Engineering, The University of Alabama, P.O. Box 870203, Tuscaloosa, Alabama 35487-0203, USA*
[2]*Department of Chemistry, University of Nebraska-Lincoln, Lincoln, Nebraska 68588, USA*

(Received 13 August 2009; accepted 5 October 2009; published online 2 November 2009)

We present density-functional theory calculations of the dehydrogenation of methane and CH_x ($x=1-3$) on a Cu/Ni(111) surface, where Cu atoms are substituted on the Ni surface at a coverage of $\frac{1}{4}$ monolayer. As compared to the results on other metal surfaces, including Ni(111), a similar activation mechanism with different energetics is found for the successive dehydrogenation of CH_4 on the Cu/Ni(111) surface. In particular, the activation energy barrier (E_{act}) for $CH \rightarrow C+H$ is found to be 1.8 times larger than that on Ni(111), while E_{act} for $CH_4 \rightarrow CH_3+H$ is 1.3 times larger. Considering the proven beneficial effect of Cu observed in the experimental systems, our findings reveal that the relative E_{act} in the successive dehydrogenation of CH_4 plays a key role in impeding carbon formation during the industrial steam reforming of methane. Our calculations also indicate that previous scaling relationships of the adsorption energy (E_{ads}) for CH_x ($x=1-3$) and carbon on pure metals also hold for several Ni(111)-based alloy systems. © *2009 American Institute of Physics*. [doi:10.1063/1.3254383]

I. INTRODUCTION AND BACKGROUND

With hydrogen as an energy carrier, fuel cells are emerging as an efficient conversion technology to produce clean and CO_2-free energy that can be used in both stationary (e.g., power plant) and mobile (e.g., vehicles) applications.[1–3] As the major component of natural gas, methane serves as an abundant resource of H_2. Given that CH_4 is highly stable due to its tetrahedral structure (Td symmetry) and noble-gas-like electron configuration with sole inert C–H σ-bonds compared to other alkanes, considerable efforts have been made (experimentally and theoretically) to elucidate the catalytic activation of the C–H bonds in CH_4, which can yield H_2 and CH_x ($x=1-3$) intermediates. Hydrogen has a wide variety of applications in industry,[2] while the CH_x species can be used as building blocks for specialty chemicals of higher value via direct conversion. However, any desirable products from the direct conversion of CH_4 are invariably more reactive than CH_4 and are subject to further reactions forming thermodynamically more stable carbon (i.e., coking) or CO_2 along the reaction path. Thus, $CO+H_2$ (syngas) is commonly desired as the protected CH_x ($x=1,2,3$) species from CH_4 for further catalytic processing (i.e., via an indirect route) to form hydrocarbons by Fischer–Tropsch synthesis and various oxygenates (e.g., methanol, formaldehyde, higher alcohols) as fuels and chemicals.

The primary process in industry to produce syngas is the steam reforming of methane (SRM), $CH_4+H_2O \rightarrow CO+3H_2$, using a Ni-based catalyst at ~30 atm and >800 °C, where the water-gas shift reaction, $CO+H_2O \rightarrow CO_2+H_2$, is the most important coexisting reaction.[4,5] However, Ni also catalyzes the formation of various carbon species (e.g., graphene, nanotubes, whiskerlike and encapsulated carbon, and pyrolytic carbon), leading to catalyst coking, which can destabilize industrial operations and deteriorate the activity of the catalyst.[5] In practice, alkali metal promoters, such as potassium, are integrated into the catalyst structure to alleviate carbon deposition by (1) neutralizing acidic sites that catalyze the decomposition of hydrocarbons and (2) preoccupying the step and defect sites that contribute significantly to carbon formation, but the side effect is a reduction in the reforming rate.[4–8] Sulfur, a catalytic poison that is unable to be completely removed from the CH_4 feedstock, is also found to help impede carbon formation. The H_2S adsorbates can selectively block the step and defect sites where carbon nucleation is most likely to take place.[5,7,8] In addition, the high temperatures associated with industrial SRM also favors carbon formation through various side reactions, such as

$$2CO \rightarrow C + CO_2, \tag{1}$$

$$CO + H_2 \rightarrow C + H_2O, \tag{2}$$

$$CH_4 \rightarrow C + 2H_2, \tag{3}$$

and

$$C_nH_{2n+2} \rightarrow nC + (n+1)H_2. \tag{4}$$

In practice, reactions (1) and (2) may be reversed if the appropriate conditions are chosen, which form the basis for *in situ* catalyst regeneration. For instance, a high H_2O/CH_4 ratio (≥ 2.5) is commonly applied in industrial operations to remove carbon deposits by gasification. Alkali promoters in

[a)]Electronic mail: weian@eng.ua.edu.
[b)]Electronic mail: xczeng@phase2.unl.edu.
[c)]Author to whom correspondence should be addressed. Electronic mail: hturner@eng.ua.edu.

the catalyst are also believed to help accelerate the gasification process. A few precious metals, e.g., Ru,[9–16] Rh,[17–20] Ir,[21–24] Pd,[25–28] and Pt,[29–34] and coinage metals Cu, Ag, and Au,[9] as well as Co,[35–37] have been extensively studied in the literature in order to explore their potential for hindering carbon formation during methane activation under mild reaction conditions. However, any conceivable catalyst comprised of the above precious metals is less likely to be employed in industrial-scale applications because of the tradeoff between the cost of the precious metals and the value of the end products.

As an alternative, bimetallic systems composed of M/Ni [where M denotes the second transition metal (TM)] have shown[38] improved performance in activating CH_4 [e.g., Fe/Ni(111) (Ref. 39)] and impeding carbon formation [e.g., Au/Ni(111) (Refs. 40–43) and Sn/Ni(111) (Refs. 44–49)]. It is known that copper and nickel, which have similar lattice constants (3.615 and 3.524 Å, respectively), can easily form a stable fcc NiCu alloy system. The alloy system is compositionally homogeneous, and therefore, Cu is not likely to form island structures on the Ni surface.[50] Previous experimental studies have shown that NiCu alloy catalysts with >10 at. % Cu can reduce the rate of carbon formation while still maintaining a reasonable rate of steam reforming.[51–53] Although SRM over a Ni-based catalyst is now considered a mature technology, the underlying details regarding methane dehydrogenation on the Cu/Ni bimetallic system are still unknown. The chemistry of the successive dehydrogenation reactions of methane is believed to be the key to understanding a family of related reactions, including SRM, carbon dioxide reforming of methane ($CO_2+CH_4 \rightarrow 2CO+2H_2$), partial oxidation of methane ($1/2O_2+CH_4 \rightarrow CO+2H_2$), and methane decomposition ($CH_4 \rightarrow C+2H_2$). Moreover, Ni-based catalysts have shown remarkable catalytic activity in these reactions and are relevant to many industrial applications.

In this paper, we present a systematic density-functional theory (DFT) study on the successive dehydrogenation of methane to form CH_3 (methyl), CH_2 (methylene), CH (methylidyne), and C on a well-defined Cu/Ni(111) surface. The energetics of the reactants, products, and transition states (TS) have been carefully examined using spin-polarized DFT and a periodic slab model. The searches for the TSs along the minimum-energy pathway (MEP) were computed using the climbing-image nudged elastic band (CI-NEB) method. As a comparison, results from other M-Ni(111) systems, e.g., M =Bi, Ag, Au, and Co, are also presented. Our DFT calculations predict that the activation energy barriers (E_{act}) for the successive dehydrogenation reactions of CH_4 are all increased due to the incorporation of Cu atoms into the Ni(111) surface. More importantly, the E_{act} for $CH \rightarrow C+H$ is predicted to increase the most. This result provides a reasonable explanation for the beneficial effect of Cu on the SRM reaction since a higher activation barrier for this final reaction would help prevent carbon formation. In addition, our DFT results reveal that the previous scaling relationships for the adsorption energy (E_{ads}) of CH_x ($x=1-3$) and carbon on pure metals also hold for the bimetallic M/Ni(111) alloy systems studied here. Finally, our calculations emphasize the importance of surface relaxation during the modeling procedure since even slight distortions in the catalyst structure play a critical role in accurately predicting the reaction energetics.

It should be noted that the realistic catalyst for SRM is a complex system in which terrace sites as well as various defects, including kinks and step sites, contribute to the activity of the catalyst. Our computational study is solely based on a model catalyst, i.e., the Cu/Ni(111) surface. In addition, there are certain factors present in the experiments that cannot be easily incorporated into theoretical simulations, such as thermal effects, detailed adsorbate-adsorbate interactions, the complex structures in real catalysts, and multiple reaction pathways from a number of reaction intermediates [e.g., CH_x^* ($x=1-3$), H^*, OH^*, CO^*, etc.] in realistic SRM. The aim of this study is not to capture all of the experimental complexities. Instead, our calculation procedure is intended to isolate the effects of Cu incorporation into a Ni(111) catalyst on the primary SRM reactions using a rigorous computational approach. Very recently, a computational study has attempted to address thermochemistry and kinetics of SRM on Ni (111) under realistic reaction conditions.[54] While this type of analysis is beyond the scope of our work, it illustrates the steps needed to bridge the gap between theoretical and experimental studies.

II. COMPUTATIONAL METHODS

All of the DFT calculations in this study were carried out using the Vienna *ab initio* simulation package.[55–57] Specifically, the spin-polarized exchange-correlation functional with generalized gradient approximation (GGA) of Perdew, Burke, and Ernzerhof (PBE) (Ref. 58) combined with the projector-augmented wave method[59] were used to solve the Kohn–Sham equations. The conjugate-gradient algorithm was adopted during the ionic relaxation to minimize the total energy. The Kohn–Sham orbitals are expanded in a plane-wave basis set with a kinetic energy cutoff of 400 eV. The $p(2\times2)$ lateral supercell was sampled with a $5\times5\times1k$-point mesh generated via the Monkhorst–Pack scheme, leading to 13 irreducible k-points in the Brillouin zone. The convergence threshold was set to be 10^{-4} eV for the total energy in the electronic self-consistent loop and 10^{-2} eV/Å of force on each atom. The first-order Methfessel–Paxton smearing[60] with $k_BT=0.2$ eV was used for partial occupancies around the Fermi level to speed up the convergence. However, all reported energies were extrapolated to $k_BT=0$ eV.

The surface was modeled by a four-layer Ni(111) slab with the lower two layers fixed at their equilibrium bulk phase positions, with a lattice constant of 3.522 Å, while the upper two layers were allowed to relax. The dehydrogenation of methane was only allowed to occur on the upper side of the slab. The two successive slabs were separated by a 13 Å vacuum region to ensure that the adsorbates and the subsequent slab would not interact. The Cu/Ni(111) surface alloy was built by substituting one Ni atom with one Cu atom on the topmost layer in the optimized $p(2\times2)$ lateral supercell, leaving each Ni atom on the surface with two Cu neighbors and four Ni neighbors (i.e., $\theta=1/4$ ML in terms of Cu cov-

erage). NiCu catalysts with Cu concentrations up to 50% have demonstrated the highest reforming/coking rate, though the exact surface concentration of Cu is unknown.[51,53,61] The Cu/Ni(111) surface was then relaxed using the same procedures as the Ni(111) surface. The adsorption energy (E_{ads}) in this work is defined as $E_{ads}=E_{total}[slab]+E_{total}[fragment]-E_{total}[slab+fragment]$, where E_{total} is the total energy of the system in one supercell. The MEP and the search for the TSs were computed using the CI-NEB method.[62] It is known that many bimetallic (M1 and M2) surface structures can adopt either the surface M1-M2-M2 or the subsurface M2-M1-M2 structures, where M1 is the admetal and M2 is the host metal. The relative thermodynamic stability of the two can vary based on the nature of the adsorbates.[63] Our calculations show that the Cu–Ni–Ni surface structure is energetically more stable (by 0.02 eV/atom) than the subsurface Ni–Cu–Ni structure, which may arise from the segregation of the admetal. The relative stability remained unchanged in the presence of the CH_x (x=0–3) and H adsorbates considered in this study. Thus, the surface model employed in this study is predicted to be representative of the general surface structure of a Cu/Ni(111) surface alloy.

III. RESULTS AND DISCUSSION

The SRM over Ni-based catalysts has been extensively studied over the past three decades (see Refs. 5 and 64 and references therein). It is now believed that the dissociation of CH_4 into surface-bound CH_3 and H is the rate-limiting step.[65,66] For instance, if the CH_4 pressure above a Ni surface is below 10^{-5} torr, dissociative adsorption of CH_4 is not experimentally observed.[65,66] With increased pressure or temperature, the impinging CH_4 molecules can overcome the activation barrier for dissociation due to increased kinetic (translational) energy or internal thermal vibrational energy. This dissociation phenomena has been observed by molecular beam experiments (equivalent to CH_4 under high pressure), combined with surface sensitive techniques, as well as high pressure CH_4 decomposition experiments.[65–69] It has been established that the dissociation of CH_4 on a Ni surface is a direct highly activated process consistent with the high stability of the C–H bonds in CH_4. Moreover, the vibrational mode-specific reactivity of CH_4 on a Ni(100) surface has also been experimentally observed such that the reaction probability with two quanta of excitation in one C–H bond is greater than that with one quantum in two different C–H bonds.[70–73] The apparent activation energy barrier has also been experimentally estimated from sticking coefficient measurements. For example, Beebe *et al.*[74] obtained activation energy barriers (E_{act}) of 0.58, 0.28, and 0.55 eV for CH_4 dissociation on Ni(110), Ni(100), and Ni(111) surfaces, respectively. Lee *et al.*[65] obtained a similar E_{act} of 0.53 eV for CH_4 dissociation on a Ni(111) surface, where the dissociation products were identified as adsorbed CH_3 and H atoms by high resolution electron energy loss spectroscopy (HREELS). They also suggested that quantum tunneling of the H atoms could play a role in the final step of the cleavage of the C–H bond. These experiments revealed that the dissociation of methane on low-index Ni surfaces, e.g., Ni(111), Ni(100), and Ni(110), proceeds via similar kinetic processes in which both translational and vibrational excitations are the driving forces for overcoming the activation energy barrier.

On the theoretical side, considerable effort has been paid to C–H bond activation and CH_x adsorption. Cluster models were often employed in the earlier work. For example, Yang and Whitten[75] investigated the dissociative chemisorption of CH_4 on a Ni(111) surface using a three-layer 41-atom cluster model with configuration interaction calculations. They predicted an E_{act} of 0.72 eV for the dehydrogenation of CH_4 on an atop Ni site, forming coadsorbed H and CH_3 as the dissociation products at the opposite threefold hollow sites. This reaction was calculated to be exothermic by 0.12 eV. In other work, Burghgraef *et al.*[35,37] predicted a much larger E_{act} of 1.25 eV for CH_4 dissociation on a Ni_{13} cluster (endothermic by 0.31 eV) using DFT calculations. As is known, cluster models are limited by inherent boundary effects, which can be significant if the size of the cluster model is too small. Accordingly, periodic slab models within the DFT framework have also been employed to explore these reactions in more recent studies. For example, Kratzer *et al.*[43] predicted an E_{act} of 1.12 eV and an endothermicity of 0.19 eV using a periodic four-layer Ni(111) slab model from their DFT calculations with a GGA-type PBE functional, a plane-wave basis set, and the pseudopotential method. In their TS search, they also imposed certain constraints (i.e., the Ni atoms were fixed) and used only spin-restricted DFT to save computational cost. Watwe *et al.*[76] used similar methods, except that a two-layer slab model and a PW91 GGA functional was used, obtaining a larger energy barrier (E_{act}=1.32 eV) and larger endothermicity (0.42 eV). Bengaard *et al.*[5] reported a comprehensive study on steam reforming and carbon formation on a Ni catalyst using DFT calculations, combined with experimental measurements. They estimated an E_{act} of 1.04 eV (0.94 eV with zero-point energy corrections included) for CH_4 activation on a Ni(111) surface using slab model. An even smaller E_{act} of 0.9 eV was obtained by fitting the experimental data to a microkinetic model.

Apparently, there exist discrepancies in the calculated E_{act} and in the exo- and endothermicity of CH_4 dissociation on a Ni (111) surface due to the differences in models and methods employed. However, the configurations for the initial state (IS), TS, and final state (FS) on the potential energy surface are quite similar from either the cluster or the slab models. It should be noted that there is a limitation on the accuracy of the energetics data from these previous studies because surface relaxation and the spin-polarization of the Ni system were not fully taken into account.

Our results are presented in Secs. III A–III D, which are organized according to the successive dehydrogenation reactions of CH_4, CH_3, CH_2, and CH. In each subsection, the adsorption of the CH_x intermediates (i.e., IS, FS, and location of the TS) are discussed, followed by correlation of their electronic structures and scaling relationships (Secs. III E and III F, respectively).

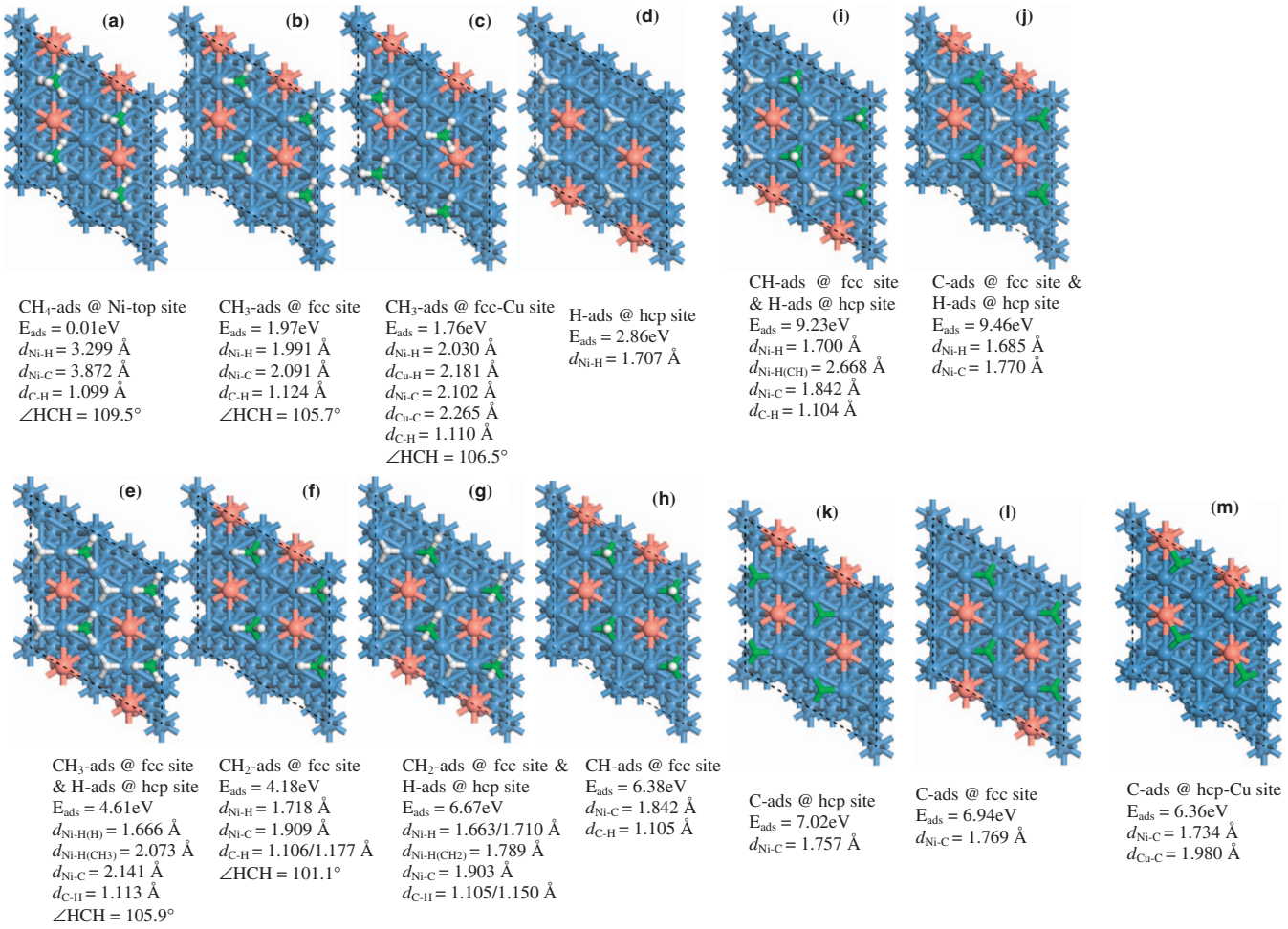

FIG. 1. Top view of CH_x (x=0–4) and H adsorbed on Cu/Ni(111) threefold hollow sites. Adsorption energy (E_{ads}), binding distance (d), and characteristic bond angle are displayed. The configurations of CH_x (x=0–3) and H coadsorption are the FSs of the corresponding CH_{x+1} (x=0–3) dehydrogenation.

A. Dehydrogenation of Methane ($CH_4 \rightarrow CH_3 + H$)

1. Adsorption of CH_4, CH_3, and H

As shown in Fig. 1(a), CH_4 is found only to physisorb on the Cu/Ni(111) surface with a negligible adsorption energy (E_{ads}) of 0.01 eV and with a long binding distance (d_{Ni-C}) of 3.872 Å, indicating a weak van-der-Waals-type interaction. This is consistent with previous calculations and experimental observations.[65,66] Thus, the incorporation of Cu atoms into Ni(111) is predicted to have little impact on CH_4 adsorption, as compared to the pure Ni(111) surface.

The dehydrogenation product, CH_3, is chemisorbed at the fcc threefold hollow site with symmetric d_{Ni-C} distances of 2.091 Å and d_{C-H} of 1.124 Å (C_{3v} symmetry). The three H atoms point toward the three Ni atoms in an eclipsed configuration [Fig. 1(b)], almost as same as that on pure Ni(111), which has been confirmed by both calculations and experimental measurements.[76,77] Similar configurations were also found on other close-packed metal surfaces, such as Rh(111).[20] The E_{ads} at the fcc threefold hollow site (1.97 eV) is slightly larger than that at the hcp threefold hollow site (1.93 eV). Thus, the CH_3 intermediate is more likely to chemisorb at the fcc site on the Cu/Ni(111) surface. Accordingly, this configuration was subsequently chosen as the IS for the next dehydrogenation step. There is a general consensus that CH_3 favors the threefold hollow site on the Ni(111) surface, where three equivalent Ni–CH_3 bonds are formed.[43,76,78] However, for CH_3 chemisorbed at the fcc-Cu site [Fig. 1(c)], the E_{ads} is reduced to 1.76 eV, suggesting that substitutionally embedded Cu atoms in the Ni(111) surface are less reactive toward CH_3 than the Ni atoms (d_{Ni-C} =2.102 Å and d_{Cu-C}=2.265 Å). Our test calculations have also shown that the relative inertness of the Cu atoms also holds for the adsorption of H, C, CH, and CH_2 on Cu/Ni(111). This is consistent with previous computational predictions that the adsorption of CH_x(x=1–3) on coinage metal surfaces, such as Cu, Ag, and Au, is generally weak.[9,26]

The H atom also prefers to chemisorb at the threefold hollow site, yielding a d_{Ni-H} of 1.707 Å and E_{ads} of 2.86 eV with C_{3v} symmetry at the hcp site [Fig. 1(d)], almost the same as that at the fcc site, E_{ads}=2.87 eV. This is the same adsorption energy as that found on pure Ni(111),[43] indicating that the H adsorption is not affected by nearest-neighbor Cu atoms. However, if the H atom is adsorbed directly at the fcc-Cu site, then the E_{ads} is reduced to 2.75 eV, with a shorter d_{Ni-H} (1.672 Å) and a longer d_{Cu-H} (1.804 Å).

When CH_3 and H coadsorb at the fcc site and the hcp site, respectively [Fig. 1(e)], the calculated E_{ads} is 4.61 eV, which is smaller than the summation of E_{ads} from CH_3 and H chemisorbed separately [E_{ads}(H)+E_{ads}(CH_3)=4.83 eV], suggesting a weakly competitive coadsorption. This is also evi-

denced by a change in the binding distances: longer d_{Ni-C} (2.141 Å versus 2.091 Å) and longer d_{Ni-H} (2.073 Å versus 1.991 Å) for adsorbed CH_3 but shorter d_{Ni-H} (1.666 Å versus 1.707 Å) for adsorbed H in the coadsorbed configuration. This configuration was thus identified as the FS of the CH_4 dehydrogenation.

2. TS of $CH_4 \rightarrow CH_3 + H$

The dissociation of CH_4 on top of a Ni atom into opposite fcc and hcp threefold hollow sites has been reported to have a lower activation energy barrier than that over a bridge site on a pure Ni(111) surface.[43,75,76] We chose gaseous CH_4 physisorbed on top of a Ni atom with four Ni atoms and two Cu atoms being the nearest neighbors [see Fig. 1(a)] as the IS and the coadsorbed CH_3 and H [see Fig. 1(e)] as the FS in the search for a TS along the MEP. It is worthy to note that such an IS represents the *naturally* adsorbed configuration, depending only on the intrinsic binding strength of CH_4 onto the catalyst surface without any external effects (e.g., temperature and pressure). As shown in Fig. 2(a), CH_3 and H in the TS are located above the Ni atom (hereafter denoted as Ni_B), which bridges the opposite fcc and hcp threefold hollow sites of $Ni-Ni_B-Ni$. The overall TS geometry is very similar to that on pure Ni(111) and Rh(111) surfaces.[17,18] Our TS structure has a calculated E_{act} of 1.41 eV, which is larger than that on pure Ni(111) surfaces mentioned previously [1.04,[5] 1.12,[43] and 1.32 eV (Ref. 76)] but smaller than that on a pure Cu(111) surface (1.7 eV).[17] Therefore, the incorporation of Cu atoms into the Ni(111) surface at $\theta = 1/4$ ML coverage hinders the activation of CH_4, similar to the effect of embedded Au atoms in Ni(111), as reported by Besenbacher *et al.*[40] and Kratzer *et al.*[43] They found an increase in E_{act} by 0.17 and 0.39 eV on Au/Ni(111) with $\theta = 1/6$ and 1/4 ML of Au coverage, respectively, compared to that on a pure Ni(111) surface. These changes were attributed to the interacting effects of neighboring Au atoms, which lower the *d*-band center of Au/Ni(111), leading to a decrease in the surface interaction with the C–H molecular antibonding orbitals. Our calculations also found that the dissociation of CH_4 on the Cu/Ni(111) surface is endothermic by 0.12 eV, which is smaller than that on a pure Ni(111) surface [0.57,[5] 0.19,[43] and 0.42 eV (Ref. 76)]. Under realistic reaction conditions the adsorption and activation of CH_4 are facilitated by high pressure (enhanced kinetic energy) and high temperature (enhanced internal thermal vibrational energy), while entropy reduction plays an adverse role. Our electronic structure calculations are only intended to yield TS structures and activation barriers corresponding to the absolute reaction condition, i.e., 0 K and zero pressure, from which only pure electronic interactions (i.e., usually the primary driving force for chemical reactions) are taken into account. The results are still relevant to the competitive or progressive reactions under realistic reaction conditions.

B. Dehydrogenation of methyl ($CH_3 \rightarrow CH_2 + H$)

The CH_x (x=1–3) species are the intermediate products from the successive dehydrogenation of CH_4, eventually leading to the formation of adsorbed carbon (x=0), which has the maximum binding energy to the catalyst surface, as compared to the other CH_x species. All of the CH_x (x=1–3) species have been experimentally observed on Ni(111) using surface sensitive techniques such as HREELS (Ref. 77) and secondary ion mass spectroscopy (SIMS),[79] suggesting that the successive dehydrogenation of methane is not a quick kinetic process, but rather sizeable activation energy barriers exist along the reaction pathway. Therefore, the energetics of the dehydrogenation of CH_x can be tuned somewhat for desirable specialty chemicals by appropriate catalyst design.

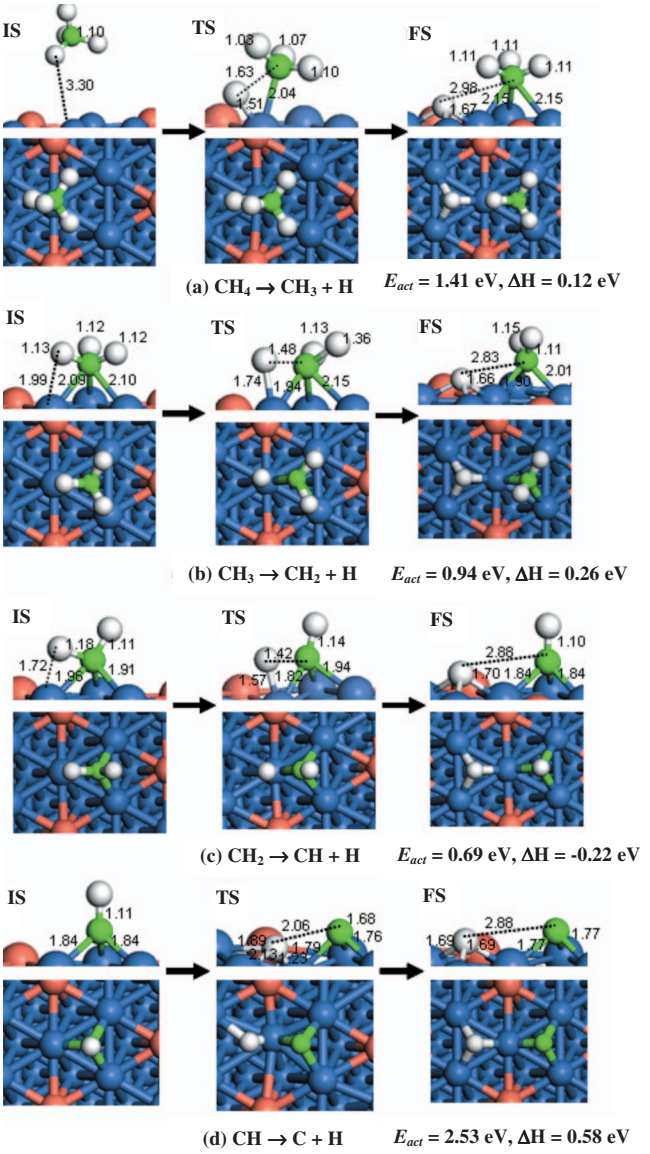

FIG. 2. IS, TS, and FS structures for the dehydrogenation of (a) methane, (b) methyl, (c) methylene, and (d) methylidyne over Cu/Ni(111). Both side (upper panel) and top (lower panel) views are displayed as well as the bond length (in angstrom) and activation energy barrier (E_{act}) and energy change between the FS and IS (ΔH).

1. Adsorption of CH_2

CH_2 prefers to chemisorb at the threefold hollow site with E_{ads}=4.18 eV at the fcc site [Fig. 1(f)], with exactly the same E_{ads} as found at the hcp site. The adsorbed CH_2 at the fcc site has one H atom pointing toward an Ni atom (d_{Ni-H}

=1.718 Å and d_{C-H}=1.177 Å) and the other H atom pointing toward the center of the Ni–Ni bridge site (d_{Ni-H}=1.909 Å and d_{C-H}=1.106 Å), leading to different activation characteristics of the two C–H bonds, evidenced by unequal d_{C-H}. A similar configuration was also found on a pure Ni(111) surface.[76]

As shown in Fig. 1(g), the coadsorption of CH_2 at the fcc site and H at the hcp site is also weakly competitive. In this case, the coadsorbed state has a total adsorption energy of E_{ads}=6.67 eV, as compared to that when CH_2 and H are chemisorbed separately [Figs. 1(f) and 1(d)], with E_{ads}=7.04 eV. This configuration was chosen as the FS for the dehydrogenation of methyl, while the CH_2 adsorbed at the fcc site [Fig. 1(f)] was chosen as the IS for the dehydrogenation of methylene.

2. TS of $CH_3 \rightarrow CH_2 + H$

As shown in Fig. 2(b), the structure of the TS corresponds to a CH_2 sitting at a fcc site and a departing H atom moving toward the top of a Ni_B atom and tilting toward the opposite hcp threefold hollow site. Compared to the adsorbed CH_3 with C_{3v} symmetry, the overall geometry of the TS looks like a heavily distorted CH_3 (d_{C-H}=1.13 Å, d_{C-H}=1.36 Å, and $d_{C\cdots H}$=1.48 Å). There is no symmetry, and the surface bond length is considerably changed: d_{Ni-C} is decreased to 1.94 Å and then increased to 2.15 from 2.09 Å in the IS. The calculated E_{act} is 0.94 eV, comparable to those [0.78,[5] 0.70,[76] and 1.04 eV (Refs. 80 and 81)] on a pure Ni(111) surface. Our calculations also show that the reaction $CH_3 \rightarrow CH_2 + H$ is endothermic by 0.26 eV. There is a large discrepancy in the calculated endothermicity of this reaction on a pure Ni(111) surface, which was calculated to be 0.03 eV by Watwe *et al.*,[76] 0.16 eV by Bengaard *et al.*,[5] and 0.50 eV by Michaelides and Hu,[80,81] where the latter two values include the effects of spin-polarization.

C. Dehydrogenation of methylene ($CH_2 \rightarrow CH + H$)

1. Adsorption of CH

As shown in Fig. 1(h), CH prefers to chemisorb at the fcc threefold hollow site with the remaining H atom oriented perpendicular to the Cu/Ni(111) surface (d_{Ni-C}=1.842 Å and d_{C-H}=1.105 Å), almost identical to the CH adsorbed on a pure Ni(111) surface (d_{Ni-C}=1.83 Å and d_{C-H}=1.10 Å).[76] The adsorbed CH also has C_{3v} symmetry. The chemisorption of CH is energetically very favorable with an E_{ads} of 6.38 eV. The unchanged d_{C-H} in the adsorbed CH (as compared to the isolated CH_4) suggests that the sp^3 hybridization needed to form three equal Ni–C bonds are mainly due to the three electrons (dangling bonds) associated with the C in CH.

As shown in Figs. 1(d), 1(h), and 1(i), the coadsorption of CH at the fcc site and H at the hcp site has almost no impact on the energetics, as compared to the individual adsorption energetics (9.23 eV for coadsorption versus 9.24 eV for isolated adsorption). The coadsorption configuration was thus selected as the FS of the CH_2 dehydrogenation reaction.

TABLE I. Adsorption energy (E_{ads}, in eV) for C and CH_x (x=1–3) at the hcp threefold hollow site on the M/Ni(111) alloy surface shown in Fig. 1(k). The calculated E_{ads} for C are in bold and E_{ads} for CH_x (x=1–3) are derived from scaling relations between CH_x and C. The valency of each species is included in the parentheses.

M-Ni(111)	C(4)	CH(3)	CH_2(2)	CH_3(1)
Cu	**7.02**	5.27	3.51	1.76
Ag	**7.08**	5.31	3.54	1.77
Au	**6.60**	4.95	3.30	1.65
Co	**6.74**	5.06	3.37	1.69
Bi	**6.04**	4.53	3.02	1.51
Pure Ni(111)	**6.81**	5.11	3.41	1.70

2. TS of $CH_2 \rightarrow CH + H$

From the results in Sec. III B 2, we chose the IS to be CH_2 adsorbed at the fcc threefold hollow site [Fig. 1(f)] and the FS to be coadsorbed CH and H [Fig. 1(i)]. As seen in Fig. 2(c), the TS structure features a departing H atom moving toward the top of the Ni_B atom and tilting toward the opposite hcp threefold hollow site ($d_{C\cdots H}$=1.42 Å and d_{Ni-H}=1.57 Å). The CH remaining at the fcc threefold hollow site is slightly moved away from the IS position, i.e., 1.96 Å versus 1.82 Å and 1.91 Å versus 1.94 Å for the two corresponding d_{Ni-C}. The TS configuration is slightly different from that previously calculated for the pure Ni(111) surface ($d_{C\cdots H}$=1.60 Å and d_{Ni-H}=1.50 Å).[76] The calculated E_{act} is 0.69 eV, over twice as large as that on a pure Ni(111) surface [0.31 eV (Ref. 5) and 0.29 eV (Ref. 76)]. This reaction was calculated to be exothermic by 0.22 eV, smaller than that [exothermic by 0.29 eV (Ref. 5) and 0.45 eV (Ref. 76)] on pure Ni(111). Apparently, the embedded Cu atoms in Ni(111) hinder the dehydrogenation of CH_2 as compared to the pure Ni(111) surface.

D. Dehydrogenation of methylidyne ($CH \rightarrow C + H$)

As the last step of the successive dehydrogenation of CH_x, the dehydrogenation of CH is of particular importance. In principle, all of the CH_x (x=1–3) species can potentially serve as the chemical feedstock for the synthesis of other desirable chemicals, such as methanol, formaldehyde, ethylene, acetylene, and aromatics if carbon formation can be blocked. In order to block the carbon formation, the activation barrier for the final dehydrogenation step must be elevated.

1. Adsorption of C

As shown Figs. 1(k) and 1(l), the C prefers to chemisorb at either the fcc or the hcp threefold hollow sites with C_{3v} symmetry. The adsorbed C has E_{ads} of 7.02 eV and d_{Ni-C} of 1.757 Å at the fcc site, while at the hcp site it has E_{ads} of 6.94 eV and d_{Ni-C} of 1.769 Å. Our calculated E_{ads} for C adsorbed on a pure Ni(111) surface is 6.74 eV at the fcc site and 6.81 eV at the hcp site. As is apparent, the incorporation of Cu into the Ni(111) surface enhances the adsorption of C, which is the opposite effect found for Au.[40–43] As shown in Table I, Bi and Co have effects that are similar to Au, while Ag shows behavior similar to Cu. When C is adsorbed at the

hcp-Cu site [Fig. 1(m)], the E_{ads} is decreased to 6.36 eV, and the adsorbed C is repelled to the bridge site of Ni–Ni with d_{Ni-C} of 1.734 Å and d_{Cu-C} of 1.980 Å. This suggests that C is more likely to deposit at the threefold hollow site of Ni–Ni–Ni instead of Ni–Ni–Cu. As the Cu coverage is increased, the number of Ni–Ni–Ni sites is decreased, leading to less stable adsorption of C on the Ni surface. As shown in Figs. 1(d), 1(j), and 1(l), the coadsorption of C at the fcc site and H at the hcp site is also weakly competitive (E_{ads} =9.46 eV), as compared to that when C and H are chemisorbed separately (E_{ads}=9.80 eV).

It has been commonly observed that for carbon fragments adsorbed on pure TM surfaces, tetravalency is preferred such that CH_3 would adsorb strongest at the atop site, CH_2 at a bridge site, and CH at a threefold hollow site.[28,82] In stark contrast, CH_x (x=1–3) all prefer the Ni–Ni–Ni threefold hollow site, where each Ni atom has two Cu neighbors at 1/4 ML of Cu coverage, suggesting the adverse effect of Cu on the adsorption of the carbon fragments.

2. TS of CH→C+H

We chose the CH adsorbed at the fcc threefold hollow site [Fig. 1(h)] as the IS and the coadsorbed H and C [Fig. 1(j)] as the FS. Prior to reaching the TS shown in Fig. 2(d), H first moves to the atop position of the Ni_B atom (d_{Ni-H} =1.80 Å and d_{C-H}=1.17 Å). At the same time, the C atom stays at the fcc site, closer to the Ni_B atom (d_{Ni-C}=1.81 and 1.84 Å), forming an intermediate structure with a smaller E_{act} of 0.84 eV.

To form the TS structure, the dissociated H further migrates toward the Ni_B–Ni bridge site (d_{Ni-H}=1.23 and 1.89 Å and $d_{C\cdots H}$=2.06 Å), with the C atom remaining at the fcc threefold hollow site (d_{Ni-C}=1.76 Å) [Fig. 2(d)]. It is important to note that severe deformation of the Ni surface structure at the reactive site is predicted, but that the flat Ni surface structure is eventually recovered in the FS configuration. This TS geometry is significantly different from that on a pure Ni(111) surface (d_{Ni-H}=1.49 Å and $d_{C\cdots H}$=1.77 Å),[76] and it has an imaginary frequency of 1300 cm^{-1}, which mainly arises from the dissociated H atom. Our frequency calculations confirm that the dissociated H atom can easily diffuse to the hcp threefold hollow site, leading to the FS structure. The calculated E_{act} is 2.53 eV, about 1.8 times larger than that on a pure Ni(111) surface [1.40 eV (Ref. 5) and 1.44 eV (Ref. 76)], while the E_{act} of $CH_4 \rightarrow CH_3+H$ on the Cu/Ni(111) surface is about 1.3 times larger than that on a pure Ni(111) surface[5,43,76] (Sec. III A 2). Our calculated results could explain the experimental observations that the relative specific reaction rate of SRM versus carbon formation is increased with respect to the concentration of Cu (up to 50%) in a NiCu catalyst.[51–53] The reaction CH→C+H is calculated to be endothermic by 0.58 eV on the alloy surface, contrary to that (exothermic by 0.45 eV) on a pure Ni(111) surface, as reported by Watwe *et al.*[76] The significance of CH→C+H in the path of methane dehydrogenation, as suggested by our calculations, agrees well with the very recent finding that CH is the most important carbon-containing intermediate in the SRM reaction system under realistic reaction conditions.[54] In addition, these results highlight the need for surface relaxation during the calculation procedure, as more restrictive geometric constraints would certainly result in skewed energy predictions.

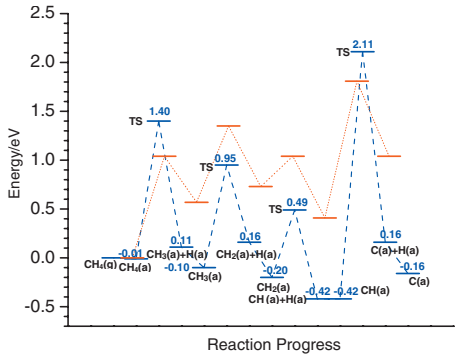

FIG. 3. Schematic energy profile for the successive dehydrogenation of CH_4 over Cu/Ni(111) from Fig. 2 is shown in blue. All energies are relative to CH_4 in the gas phase. Energy for adsorbed CH_x (x=0–3) species is referred to as the sum of adsorbed CH_x and (4−x) of H diffused to an equivalent site far from CH_x. As a comparison, the energy profile over pure Ni (111) is replotted in red from Ref. 5.

In the end, the schematic energy profile for the successive dehydrogenation of CH_4 over Cu/Ni(111) is plotted in Fig. 3 to provide an overview of the reaction pathway. In addition, Table II summarizes our DFT predictions on the Cu/Ni(111) alloy surface versus other metals. For the pure Ni(111) surface, we list DFT results from Ref. 5 since the methods and models used by Bengaard *et al.* are among the more reliable ones used in the literature.

As a further comparison, we also conducted a search for the TS of CH→C+H on the Bi/Ni(111) surface (Fig. 4) using the same procedures as for the Cu/Ni(111) surface. However, the TS is significantly different from that on either Ni(111) or Cu/Ni(111). On the Bi/Ni(111) surface, the C atom moves to the atop position of the Ni atom, forming multiple bonds with Ni and Bi (d_{Ni-C}=1.86 Å and d_{Bi-C} =2.46 Å), and the H atom moves to the nearby fcc-Bi three-

TABLE II. Comparison of the activation energy barrier (E_{act}, in eV) for the successive dehydrogenation of CH_4 on Cu/Ni(111) (in bold), Ni(111), Ni(211), Rh(111), Ru(0001), Pd(100), Pt(110), and Rh/Cu (111) surfaces. Data shown for Ni(111) and Ni(211) have been interpolated from Fig. 1 in Ref. 5.

Reaction	Cu/Ni(111)	Ni(111)	Ni(211)	Rh(111)	Ru(0001)	Pd(100)	Pt(110)	Rh/Cu(111)
$CH_4 \rightarrow CH_3+H$	**1.41**	1.04	0.83	0.69	0.88	0.79	0.35	0.70
$CH_3 \rightarrow CH_2+H$	**0.94**	0.78	0.62	0.42	0.51	0.52	0.34	0.84
$CH_2 \rightarrow CH+H$	**0.69**	0.31	0.47	⋯	0.17	0.20	0.56	⋯
$CH \rightarrow C+H$	**2.53**	1.40	0.93	⋯	1.12	0.52	1.20	⋯
Reference	**This work**	Reference 5	Reference 5	Reference 17	Reference 12	Reference 27	Reference 32	Reference 17

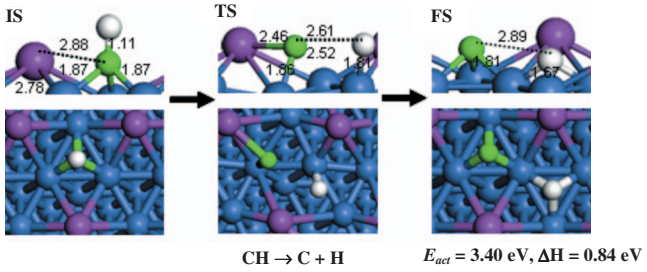

FIG. 4. IS, TS, and FS structures for the dehydrogenation of methylidyne over Bi/Ni(111), as in Fig. 2.

fold hollow site (d_{Ni-H}=1.81 Å). Due to the inertness of Bi toward C and H radicals, the C and H atoms further diffuse to the fcc and hcp threefold hollow sites of Ni–Ni_B–Ni, respectively, leading to the FS structure. The calculated activation energy barrier for the dehydrogenation of CH on the Bi/Ni(111) surface is surprisingly high, E_{act}=3.40 eV (with an endothermicity of 0.84 eV), which could explain the experimental finding that increased Bi concentration significantly inhibits carbon formation.[83]

For comparison, the numerical values of E_{act} are collected in Table II for the successive dehydrogenation of CH_4 on the low-index metal surfaces of Ni(111), Ni(211), Rh(111), Ru(0001), Pd(100), Pt(110), Rh/Cu(111), and Cu/Ni(111), which have been obtained from the literature and from our calculations. Indeed, the activation energy barrier for $CH_4 \rightarrow CH_3+H$ on the noble metal surfaces is much lower than that on the Ni-based catalyst, indicating the high activity of noble metals for activating methane. Unfortunately, these high-performance catalysts are not often practical in industrial applications because of their high costs. Nickel-based catalysts, however, can be improved by modifying the local structure and the chemical composition at the reaction site so that the catalyst characteristics can be tuned for desirable products and for enhanced catalytic durability.

E. Density of states for surface atoms

In Fig. 5, we show the projected–density of states (DOS) for the surface atoms of Ni, Cu, and Bi, as well as C–H_{dis} (where H_{dis} denotes the dissociated H atom) in the TS structure and C–H in the free CH_4 and CH species. It can be seen that the *d*-states of the surface Ni atoms on Cu/Ni(111) are only slightly changed due to the embedded Cu atoms, as compared to that on Ni(111) [Fig. 5(a)]. However, the *d*-states of the surface Cu atoms are pronounced below the Fermi level (E_F), leading to strong overlaps with the *d*-states of the surface Ni atoms below E_F, down to −5 eV. This could explain the formation of the homogeneous NiCu surface alloy with strong NiCu bonding interactions. The *s*- and *p*-states of C–H in the free CH_4 and CH [Figs. 5(f) and 5(g)] are broadened into resonances at the energy range of −9 ~ −6 eV and shifted down due to their interactions with the *d*-states of the surface Ni atoms, filling up the antibonding states of CH_4 and CH [Figs. 5(b), 5(c), and 5(e)]. There exist only weak interactions between the *s* and *p*-states of C–H_{dis} and the *d*-states of the surface Ni atoms in the TS of $CH_4 \rightarrow CH_3+H$ [Fig. 5(b)], whereas, there exist larger overlaps

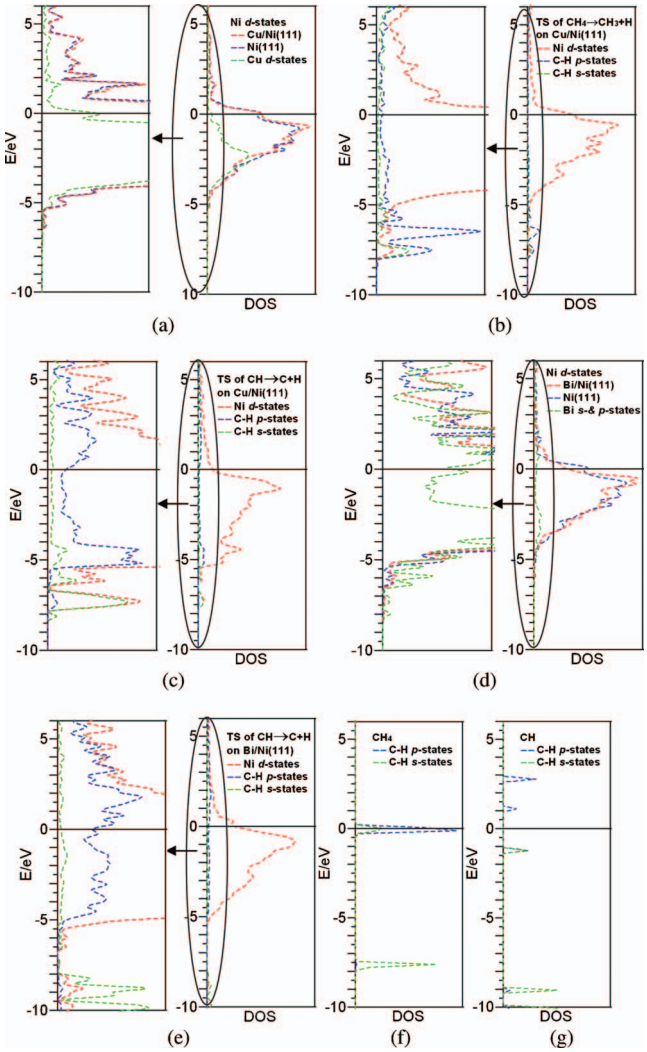

FIG. 5. Projected-DOS for surface atoms of Ni, Cu, and Bi as well as C–H_{dis} (H_{dis} denotes the dissociated H atom) in the TS structure and for C–H in free CH_4 and CH. (a) Free Cu/Ni(111). (b) TS on Cu/Ni(111). (c) TS on Cu/Ni(111). (d) Free Bi/Ni(111). (e) TS on Bi/Ni(111). (f) Free CH_4. (g) Free CH. The *d*-states of Ni and Cu, *s*- and *p*-states of Bi and C–H are drawn in the plot. The DOS of (a)–(e) are drawn at the same scale, and (f) and (g) are drawn at the same scale. The enlargements of detailed DOS are also shown. The line at 0 eV denotes Fermi level.

between the *s* and *p*-states of C–H_{dis} and the *d*-states of the Ni atoms in the TS of CH→C+H at around −4 ~ −5.5 eV below E_F [Fig. 5(c)]. A similar pattern can also be seen for Bi/Ni(111) and the TS of CH→C+H on the Bi/Ni(111) surface [Figs. 5(d) and 5(e)].

According to the *d*-band model by Hammer and Norskov,[84,85] the *d*-band center of similar TM systems closely correlates with the TM's general catalytic activity, such that the reactivity of the TM increases (or the activation energy barrier decreases) as the position of the *d*-band center is shifted upward.[85] Very recently, Nikolla *et al.*[46] demonstrated that the critical shifts in the *d*-band center in Sn/Ni(111) are directly related to the formation of new electronic states induced by Sn. Their theoretical studies, combined with state-of-the-art experimental techniques, provide direct evidence of the structure-performance relationship in SRM on a NiSn alloy catalyst. Indeed, if the projected-DOS for Bi/Ni(111) is closely examined

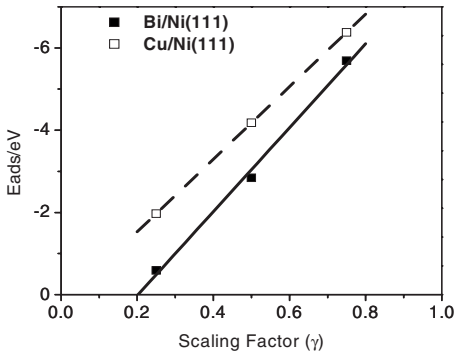

FIG. 6. Calculated adsorption energy (E_{ads}) of CH_x (x=1–3) intermediate at the fcc threefold hollow site on the Cu/Ni(111) and Bi/Ni(111) alloy surfaces shown in Fig. 1(b) as a function of the scaling factor (γ) of CH_x, where γ=0.75 if x=1, γ=0.50 if x=2, and γ=0.25 if x=3.

[Fig. 5(d)], the *d*-band of the surface Ni is slightly broadened (red line) and shifted downward. This is due to the *s*- and *p*-states of embedded Bi (green line) above and below the Fermi level, as compared with that for the pure Ni(111) surface (blue line). However, for Cu/Ni(111), such shifts in the *d*-band center are challenging to distinguish [see Fig. 5(a)]. In addition, the TMs can often undergo sizeable surface reconstruction along the reaction pathway, by which the activation energy barrier can be altered. The deformation of the surface structure can be significant, as seen in Fig. 2(d), which corresponds to the reaction CH→C+H. This deformation makes it difficult to clearly correlate the E_{act} of the TS with the E_{ads} of the FS.

F. Scaling relations on the alloy surfaces

Abild-Pedersen *et al.* developed and applied a scaling relationship to predict the trends in the catalytic activity of different TMs for AH_x intermediates and A (where A =C,N,O).[82,86–89] By performing a series of DFT calculations for a large number of adsorbates and TM surfaces, they discovered that the adsorption energy for molecules of the type AH_x is linearly correlated with the adsorption energy of atom A, i.e., $E_{ads}(AH_x)=\gamma(x)E_{ads}(A)+\xi$, where the slope $\gamma(x)$ is defined as the scaling factor and ξ is a fitted parameter. This factor can be calculated as $(x_{max}-x)/x_{max}$, where x_{max} is the maximum number of H atoms that can bond to atom A in order to form a neutral gas-phase molecule, according to the octet rule (e.g., $x_{max}=4$ for A=C and γ =0.75 if x=1; also see Fig. 6). The scaling behavior can be viewed as an illustration of bond order conservation.

Our calculations reveal that the scaling relationship of E_{ads} for CH_x (x=1–3) and C also hold for the M-Ni(111) alloy catalysts studied here, as demonstrated by the linear correlation between the calculated E_{ads} and the scaling factor in Fig. 6. Based on the calculated E_{ads} of C and the scaling relationship with CH_x (x=1–3), we obtained the E_{ads} for CH_x (x=1–3) adsorbed at the hcp threefold hollow site of Ni–Ni–Ni on the M-Ni(111) alloy surface (where M=Cu, Ag, Au, Co, and Bi), as well as on the pure Ni(111) surface (see Table I).

It can be seen that the E_{ads} increases with respect to the valency of CH_x (x=0–3), which is an indicator of free bonding. The adsorption of carbon at the threefold hollow site on the Ni(111) surface is likely to be destabilized by embedding Bi, Au, and Co atoms in the nearest-neighbor adsorption site of Ni, but the carbon adsorption is stabilized by the Cu and Ag atoms. The adsorption energy is an indicator of the stability of the adsorbed species, and it can be used to predict the tendency of carbon to accumulate on the catalyst surface.[40] Indeed, carbon that is more weakly adsorbed on the Ni surface has a greater tendency to react with adsorbed O, thereby forming CO and leading to a lower coverage of carbon. However, as seen from our calculations, the relatively high activation energy barrier for CH→C+H can also lower the tendency to form carbon on the catalyst surface during the successive dehydrogenation of methane, which has been validated by experimental measurements.[51–53]

According to the scaling relations, the E_{act} for a full catalytic reaction can be estimated from a database of E_{ads} of a few atoms and molecules for one TM such as $M_1: E_{act}(AH_x)_{M_2}=E_{act}(AH_x)_{M_1}+\gamma(x)[E_{ads}(A)_{M_2}-E_{ads}(A)_{M_1}]$. Based on this scaling relation [i.e., M_1=Cu/Ni(111) and M_2=Bi/Ni(111)], we obtained the E_{act} for CH→C+H on Bi/Ni(111) to be 3.21 eV, which is quite close to that (3.40 eV) obtained from the TS search by the CI-NEB method. As is known, a catalytic surface reaction is a complex dynamic process, in which the surface reconstruction of the catalyst surface at the reactive site is essential to the progress of the reaction as shown in Sec. III D 2. While the scaling relations could oversimplify the heterogeneous catalytic reaction, such an analysis provides an efficient tool for screening through a large amount of potential catalysts based on the database of adsorption energy and one set of activation energy. Here, we report the E_{act} for the dehydrogenation of CH_3 and CH_2 on Bi/Ni(111), as estimated from the scaling relations to be 1.17 and 1.15 eV, respectively, which may serve as a reference for future studies.

IV. CONCLUSIONS

In this work, we report a DFT-based computational study on the successive dehydrogenation reactions of CH_4 on a Cu/Ni(111) bimetallic surface model. It is found that the energetics of successive CH_4 dehydrogenation is altered by substitutionally embedded Cu atoms on the Ni(111) surface, as compared to the corresponding reactions on a pure Ni(111) surface.[5] Although the trend of the activation energy remains the same as that on pure Ni(111), the activation energy barrier for CH→C+H (2.53 eV) is appreciably enhanced with respect to that for CH_4→CH_3+H (1.41 eV). Our calculations also show that the scaling relations of the adsorption energy (E_{ads}) for CH_x (x=1–3) and C also hold for M-Ni(111) alloy systems with M=Cu, Ag, Au, Co, and Bi. With respect to the adsorption of carbon at the threefold hollow site on the Ni(111) surface, substitutionally embedded atoms of Bi, Au, and Co destabilize the adsorption, whereas Cu and Ag atoms stabilize the adsorption. This reveals that besides the adsorption energy of adsorbed carbon, the relative activation energy barrier (or reaction rate) should also be taken into account when catalysts are optimized for mitigating carbon formation. Finally, our calculations illus-

trate the importance of surface relaxation during the modeling procedure due to the distortions in the catalyst structure that are encountered during certain reaction steps.

ACKNOWLEDGMENTS

Funding for this work was partially provided by a NSF CAREER Award (Grant No. 0747690). Supercomputer resources were provided by the Alabama Supercomputer Center, NCSA TeraGrid, and the Pacific Northwest National Laboratory EMSL facility.

[1] I. E. Agency, *Hydrogen and Fuel Cells: Review of National R&D Programs* (OECD, Paris, France, 2004).
[2] J. N. Armor, Appl. Catal., A **176**, 159 (1999).
[3] J. R. Rostrup-Nielsen and R. Nielsen, Catal. Rev. - Sci. Eng. **46**, 247 (2004).
[4] J. R. Rostrup-Nielsen, *Steam Reforming Catalysts* (Danish Technical, Copenhagen, 1975).
[5] H. S. Bengaard, J. K. Norskov, J. Sehested, B. S. Clausen, L. P. Nielsen, A. M. Molenbroek, and J. R. Rostrup-Nielsen, J. Catal. **209**, 365 (2002).
[6] H. S. Bengaard, I. Alstrup, I. Chorkendorff, S. Ullmann, J. R. Rostrup-Nielsen, and J. K. Norskov, J. Catal. **187**, 238 (1999).
[7] F. Abild-Pedersen, J. Greeley, and J. K. Norskov, Catal. Lett. **105**, 9 (2005).
[8] F. Abild-Pedersen, O. Lytken, J. Engbaek, G. Nielsen, I. Chorkendorff, and J. K. Norskov, Surf. Sci. **590**, 127 (2005).
[9] C. T. Au, C. F. Ng, and M. S. Liao, J. Catal. **185**, 12 (1999).
[10] H. L. Abbott and I. Harrison, J. Catal. **254**, 27 (2008).
[11] I. M. Ciobica, F. Frechard, R. A. van Santen, A. W. Kleyn, and J. Hafner, Chem. Phys. Lett. **311**, 185 (1999).
[12] I. M. Ciobica, F. Frechard, R. A. van Santen, A. W. Kleyn, and J. Hafner, J. Phys. Chem. B **104**, 3364 (2000).
[13] R. C. Egeberg and I. Chorkendorff, Catal. Lett. **77**, 207 (2001).
[14] J. H. Larsen, P. M. Holmblad, and I. Chorkendorff, J. Chem. Phys. **110**, 2637 (1999).
[15] J. M. Wei and E. Iglesia, J. Catal. **225**, 116 (2004).
[16] J. M. Wei and E. Iglesia, J. Phys. Chem. B **108**, 7253 (2004).
[17] A. Kokalj, N. Bonini, S. de Gironcoli, C. Sbraccia, G. Fratesi, and S. Baroni, J. Am. Chem. Soc. **128**, 12448 (2006).
[18] A. Kokalj, N. Bonini, C. Sbraccia, S. de Gironcoli, and S. Baroni, J. Am. Chem. Soc. **126**, 16732 (2004).
[19] C. T. Au, M. S. Liao, and C. F. Ng, Chem. Phys. Lett. **267**, 44 (1997).
[20] B. S. Bunnik and G. J. Kramer, J. Catal. **242**, 309 (2006).
[21] G. Henkelman and H. Jonsson, Phys. Rev. Lett. **86**, 664 (2001).
[22] H. L. Abbott and I. Harrison, J. Phys. Chem. B **109**, 10371 (2005).
[23] G. Henkelman, A. Arnaldsson, and H. Jonsson, J. Chem. Phys. **124**, 044706 (2006).
[24] J. M. Wei and E. Iglesia, Angew. Chem., Int. Ed. **43**, 3685 (2004).
[25] M. S. Liao, C. T. Au, and C. F. Ng, Chem. Phys. Lett. **272**, 445 (1997).
[26] M. S. Liao and Q. E. Zhang, J. Mol. Catal. A: Chem. **136**, 185 (1998).
[27] C. J. Zhang and P. Hu, J. Chem. Phys. **116**, 322 (2002).
[28] J. F. Paul and P. Sautet, J. Phys. Chem. B **102**, 1578 (1998).
[29] A. T. Anghel, D. J. Wales, S. J. Jenkins, and D. A. King, Phys. Rev. B **71**, 113410 (2005).
[30] A. Bukoski, H. L. Abbott, and I. Harrison, J. Chem. Phys. **123**, 094707 (2005).
[31] M. A. Petersen, S. J. Jenkins, and D. A. King, J. Phys. Chem. B **108**, 5909 (2004).
[32] M. A. Petersen, S. J. Jenkins, and D. A. King, J. Phys. Chem. B **108**, 5920 (2004).
[33] J. M. Wei and E. Iglesia, J. Phys. Chem. B **108**, 4094 (2004).
[34] C. J. Zhang and P. Hu, J. Chem. Phys. **116**, 4281 (2002).
[35] H. Burghgraef, A. P. J. Jansen, and R. A. van Santen, J. Chem. Phys. **101**, 11012 (1994).
[36] H. Burghgraef, A. P. J. Jansen, and R. A. van Santen, J. Chem. Phys. **103**, 6562 (1995).
[37] H. Burghgraef, A. P. J. Jansen, and R. A. van Santen, Surf. Sci. **324**, 345 (1995).
[38] A. Groß, Top. Catal. **37**, 29 (2006).
[39] H. Yang and J. L. Whitten, Surf. Sci. **289**, 267 (1993).
[40] F. Besenbacher, I. Chorkendorff, B. S. Clausen, B. Hammer, A. M. Molenbroek, J. K. Norskov, and I. Stensgaard, Science **279**, 1913 (1998).
[41] P. M. Holmblad, J. H. Larsen, I. Chorkendorff, L. P. Nielsen, F. Besenbacher, I. Stensgaard, E. Laegsgaard, P. Kratzer, B. Hammer, and J. K. Norskov, Catal. Lett. **40**, 131 (1996).
[42] P. M. Holmblad, J. H. Larsen, and I. Chorkendorff, J. Chem. Phys. **104**, 7289 (1996).
[43] P. Kratzer, B. Hammer, and J. K. Norskov, J. Chem. Phys. **105**, 5595 (1996).
[44] E. Nikolla, A. Holewinski, J. Schwank, and S. Linic, J. Am. Chem. Soc. **128**, 11354 (2006).
[45] E. Nikolla, J. Schwank, and S. Linic, J. Catal. **263**, 220 (2009).
[46] E. Nikolla, J. Schwank, and S. Linic, J. Am. Chem. Soc. **131**, 2747 (2009).
[47] S. Saadi, B. Hinnemann, S. Helveg, C. C. Appel, F. Abild-Pedersen, and J. K. Norskov, Surf. Sci. **603**, 762 (2009).
[48] E. Nikolla, J. Schwank, and S. Linic, J. Catal. **250**, 85 (2007).
[49] E. Nikolla, J. W. Schwank, and S. Linic, Catal. Today **136**, 243 (2008).
[50] A. Christensen, A. V. Ruban, P. Stoltze, K. W. Jacobsen, H. L. Skriver, J. K. Norskov, and F. Besenbacher, Phys. Rev. B **56**, 5822 (1997).
[51] J. R. Rostrup-Nielsen and I. Alstrup, Catal. Today **53**, 311 (1999).
[52] M. T. Tavares, C. A. Bernardo, I. Alstrup, and J. R. Rostrupnielsen, J. Catal. **100**, 545 (1986).
[53] C. A. Bernardo, I. Alstrup, and J. R. Rostrupnielsen, J. Catal. **96**, 517 (1985).
[54] D. W. Blaylock, T. Ogura, W. H. Green, and G. J. O. Beran, J. Phys. Chem. C **113**, 4898 (2009).
[55] G. Kresse and J. Hafner, J. Phys.: Condens. Matter **6**, 8245 (1994).
[56] G. Kresse, J. Furthmuller, and J. Hafner, Phys. Rev. B **50**, 13181 (1994).
[57] G. Kresse and J. Furthmuller, Phys. Rev. B **54**, 11169 (1996).
[58] J. P. Perdew, K. Burke, and M. Ernzerhof, Phys. Rev. Lett. **77**, 3865 (1996).
[59] G. Kresse and D. Joubert, Phys. Rev. B **59**, 1758 (1999).
[60] M. Methfessel and A. T. Paxton, Phys. Rev. B **40**, 3616 (1989).
[61] I. Alstrup, M. T. Tavares, C. A. Bernardo, O. Sorensen, and J. R. Rostrup-Nielsen, Mater. Corros. **49**, 367 (1998).
[62] G. Henkelman, B. P. Uberuaga, and H. Jonsson, J. Chem. Phys. **113**, 9901 (2000).
[63] C. A. Menning and J. G. G. Chen, J. Chem. Phys. **130**, 174709 (2009).
[64] J. R. Rostrup-Nielsen, J. Sehested, and J. K. Norskov, Adv. Catal. **47**, 65 (2002).
[65] M. B. Lee, Q. Y. Yang, and S. T. Ceyer, J. Chem. Phys. **87**, 2724 (1987).
[66] M. B. Lee, Q. Y. Yang, S. L. Tang, and S. T. Ceyer, J. Chem. Phys. **85**, 1693 (1986).
[67] S. T. Ceyer, J. D. Beckerle, M. B. Lee, S. L. Tang, Q. Y. Yang, and M. A. Hines, J. Vac. Sci. Technol. A **5**, 501 (1987).
[68] P. M. Holmblad, J. Wambach, and I. Chorkendorff, J. Chem. Phys. **102**, 8255 (1995).
[69] L. Hanley, Z. Xu, and J. T. Yates, Surf. Sci. **248**, L265 (1991).
[70] R. D. Beck, P. Maroni, D. C. Papageorgopoulos, T. T. Dang, M. P. Schmid, and T. R. Rizzo, Science **302**, 98 (2003).
[71] P. Maroni, D. C. Papageorgopoulos, M. Sacchi, T. T. Dang, R. D. Beck, and T. R. Rizzo, Phys. Rev. Lett. **94**, 246104 (2005).
[72] L. B. F. Juurlink, R. R. Smith, D. R. Killelea, and A. L. Utz, Phys. Rev. Lett. **94**, 208303 (2005).
[73] D. R. Killelea, V. L. Campbell, N. S. Shuman, and A. L. Utz, Science **319**, 790 (2008).
[74] T. P. Beebe, D. W. Goodman, B. D. Kay, and J. T. Yates, J. Chem. Phys. **87**, 2305 (1987).
[75] H. Yang and J. L. Whitten, J. Chem. Phys. **96**, 5529 (1992).
[76] R. M. Watwe, H. S. Bengaard, J. R. Rostrup-Nielsen, J. A. Dumesic, and J. K. Norskov, J. Catal. **189**, 16 (2000).
[77] Q. Y. Yang, K. J. Maynard, A. D. Johnson, and S. T. Ceyer, J. Chem. Phys. **102**, 7734 (1995).
[78] H. Yang and J. L. Whitten, J. Am. Chem. Soc. **113**, 6442 (1991).
[79] M. P. Kaminsky, N. Winograd, G. L. Geoffroy, and M. A. Vannice, J. Am. Chem. Soc. **108**, 1315 (1986).
[80] A. Michaelides and P. Hu, J. Chem. Phys. **112**, 6006 (2000).
[81] A. Michaelides and P. Hu, J. Chem. Phys. **112**, 8120 (2000).
[82] F. Abild-Pedersen, J. Greeley, F. Studt, J. Rossmeisl, T. R. Munter, P. G. Moses, E. Skulason, T. Bligaard, and J. K. Norskov, Phys. Rev. Lett. **99**, 016105 (2007).
[83] D. L. Trimm, Catal. Today **37**, 233 (1997).
[84] B. Hammer and J. K. Norskov, Surf. Sci. **343**, 211 (1995).

[85] B. Hammer, Top. Catal. **37**, 3 (2006).
[86] G. Jones, T. Bligaard, F. Abild-Pedersen, and J. K. Norskov, J. Phys.: Condens. Matter **20**, 064239 (2008).
[87] G. Jones, J. G. Jakobsen, S. S. Shim, J. Kleis, M. P. Andersson, J. Rossmeisl, F. Abild-Pedersen, T. Bligaard, S. Helveg, B. Hinnemann, J. R. Rostrup-Nielsen, I. Chorkendorff, J. Sehested, and J. K. Norskov, J. Catal. **259**, 147 (2008).
[88] F. Studt, F. Abild-Pedersen, T. Bligaard, R. Z. Sorensen, C. H. Christensen, and J. K. Norskov, Science **320**, 1320 (2008).
[89] E. M. Fernandez, P. G. Moses, A. Toftelund, H. A. Hansen, J. I. Martinez, F. Abild-Pedersen, J. Kleis, B. Hinnemann, J. Rossmeisl, T. Bligaard, and J. K. Norskov, Angew. Chem., Int. Ed. **47**, 4683 (2008).